Sādhanā Vol. 28, Parts 3 & 4, June/August 2003, pp. 763–782. © Printed in India

Convergent beam electron diffraction – A novel technique for materials characterisation at sub-microscopic levels

M VIJAYALAKSHMI, S SAROJA and R MYTHILI

Physical Metallurgy Section, Materials Characterisation Group, Indira Gandhi Centre for Atomic Research, Kalpakkam 603 102, India
e-mail: mvl@igcar.ernet.in

Abstract. This paper presents a review of the developments in Convergent Beam Electron Diffraction (CBED), a technique widely used for determination of structure, symmetry details and atom positions in a crystal as small as 20Å in size. The understanding of this technique is related to the rapid advancements in the field of transmission electron microscopy with respect to development of coherent, finer probes and electron optics for higher spatial resolution. Energy filtering devices enable imaging of several finer features in the CBED pattern from which useful information about a crystal can be obtained. These include (i) three-dimensional information about the reciprocal lattice, (ii) point and space group symmetry details, (iii) lattice parameter from regions as fine as 2 nm, (iv) atom positions within a unit cell and (v) defects in crystals and (vi) thickness. Due to abundant data obtained from microscopic regions, this technique is unique and finds wide application in materials characterization. It has been used for studying problems like identification of the presence of lattice strain, identification of point defects etc. in a material used often in the nuclear industry, namely 9Cr–1Mo steel. The present paper provides the current status of CBED starting from its historical development, the information that can be obtained and its use in a variety of applications.

Keywords. Convergent beam electron diffraction; nanodiffraction; holography; reciprocal lattice, lattice parameter; convergence angle.

1. Introduction

Convergent beam electron diffraction, generally referred to as CBED, is one of the most powerful techniques for the determination of crystal structure in the field of transmission electron microscopy (TEM). This technique is used for fingerprinting crystals as fine as 20Å, by determining a number of parameters ranging from the symmetry of the crystal to the position of atoms within the unit cell of the diffracting crystal. The technique of CBED was discovered in 1939 by Kossel & Mollenstedt (1939), who obtained remarkably good patterns, especially considering that they had to work with large probes, with small convergence angles. The subsequent development of STEM units made it possible to obtain finer probes with larger angles of convergence, making CBED more popular. Concurrently, development of coherent, powerful electron sources like the LaB_6, field emission and field ion guns (Crewe &

Eggenberger 1968), improved design of etc. lens systems with less aberration, imaging using energy filtering devices (Lanio 1986) etc. have made this technique very powerful. Parallel concerted efforts were focused on the understanding of the principle of imaging, the origin of fine, additional features that appear in CBED patterns and methods to extract additional details about the crystal using this information. In fact, the major and long standing drawback of electron diffraction, in comparison with X-ray or neutron diffraction, with respect to its inability to identify the position of atoms in a unit cell, was completely eliminated by the development of CBED. The journey through the exciting evolution of this technique in the later half of the previous century is very interesting.

The present paper provides a review of the fascinating developments in the area of CBED. The paper is formulated into the following sub-sections: (a) Historical perspective of the developments in CBED, (b) basic principles, (c) additional information in CBED and (d) present status.

2. Historical perspective of the developments in CBED

Convergent beam electron diffraction is a technique with a long history of gradual development which has recently become widely available through the development of commercial TEM/STEM electron microscopes. Trials for detailed understanding of the concept of convergent beams were made by G Mollenstedt by building his own convergent beam electron diffraction camera operating at a voltage of 45 kV (Kossel & Mollenstedt 1939). It used a wine bottle as the electron source. The vacuum at the specimen was 10^{-3} torr and the probe size was about 40 μm. With such a large probe, contamination was not a problem despite a poor vacuum. Using flakes of mica as samples, he obtained very good CBED patterns.

For the first two decades, about from the 1940's to the 60's most of the efforts in TEM were towards developing the capability of the microscopes by improving their design features. The progress in CBED development was rather slow and emphasis was mainly on the theoretical development. MacGillavry (1940) used the two-beam theory to fit experimental CBED patterns in the first attempt to measure structural factors using dynamical electron diffraction theory. In the 1950's, theoretical work on the dynamical theory was continued by many researchers, and Kambe (1957) showed in his study on the three-beam theory that intensity of diffracted beams depends on the sum of structural factors and could be measured. Throughout the sixties, the CBED method was developed by Lehmpfuhl in Berlin (Lehmpfuhl & Reissland 1968), by Goodman (Goodman & Lehmpfuhl 1968) and by Moodie (1972) in Melbourne with the old, unsatisfactory microscopes. Gjonnes & Moodie (1965) explained the occurrence of forbidden reflections in the presence of strong multiple scattering, which could be used to identify the translational symmetry elements. During this period, Uyeda and Hoier showed how the position of Kikuchi lines can be used to determine accelerating voltages and lattice constants (HOLZ lines in CBED patterns). At about the same time Uyeda (1968) and Watanabe (Watanabe *et al* 1968) in Japan discovered the critical voltage effect* on Kikuchi lines. Gjonnes & Hoier (1971) analysed this effect based on the three-beam theory

*This is the most accurate method for structure factor determination by the electron diffraction technique. Using an electron microscope with variable accelerating voltage, it is possible to observe a minimum of intensity in the second-order reflection at the Bragg condition for a particular voltage called the critical voltage, which is sensitive to the ratio of first- to second-order structure factors.

and showed that the absence of intensity at certain points in these patterns may be used to determine the three-phase invariant for centro-symmetric crystals. Thus it may be said that most of the important theoretical development of CBED was during the sixties.

By the early seventies, electron microscopes with very good design features like STEM, modified attachments, probes etc. had developed. An excellent review on the developments in electron microscopy is presented by Newbury & Williams (2000). During the same period, systematic procedures for determination of point and space group symmetry by CBED had begun to emerge due to the work by Goodman & Lehmpfuhl (1968), Steeds (1979) and Buxton *et al* (1976). The theoretical foundations for point-group determination were established by Buxton and coworkers in the context of group theory who also developed the perturbation theory for HOLZ interactions. In 1984, the fruitful result of the focused effort of Steeds group in Bristol was the publication of an atlas of CBED patterns for various alloy phases (Steeds & Mansfield 1984). Starting from 1985, the high quality work of Tanaka's group in Japan produced excellent CBED patterns covering a wide range of applications and case studies (Tanaka & Terauchi 1985; Tanaka *et al* 1988).

Ever since the applications of CBED have been growing. It is worthwhile recalling a few of them now. The Bristol group's study on phase transformations in layer compounds supporting charge-density waves brought the CBED technique to the attention of solid state physicists for the first time. The group was also successful in the structure determination of AuGeAs by CBED (Vincent *et al* 1984). At the same time, the technique was popularized in the US by the renowned work of Eades (1984) at Illinois. Throughout the late seventies and early eighties, Cowley in Arizona was developing the coherent CBED method using sub-nanometre probes to study regions of a crystal smaller than a unit cell (Cowley 1978a). Similar work on nanodiffraction, using imaging energy filters and novel detectors was later developed by Brown and co-workers in UK, which facilitated the study of defects in crystals (Brown *et al* 1988). The use of CBED patterns to study line and planar defects also first began to be studied at about this time. Large angle CBED (LACBED) for HOLZ and ZOLZ reflections were then developed in 1985 by Tafto and co-workers (Tafto & Metzger 1985). HOLZ effects from artificial super lattices appeared first in the work of Cherns *et al* (1988). The value of shadow-imaging in CBED of HOLZ line intensities were realized during this period.

Research on structure factor phase measurements in non-centro symmetric crystals was begun in the mid-1980's by Marthinsen, Hoier (1986, 1988) and others. Zoo *et al* (1989) were successful in experimental structure–factor phase measurements, with accuracy better than one degree. At about the same time, measurements of local strains began to appear, reflected by the position of HOLZ lines with various dynamical correction schemes based on the previous theoretical work by Jones and others (Jones & Hoier 1969) on dynamical shifts on Kikuchi lines.

Quantitative analysis of CBED patterns has become accurate after the use of elastic energy filtering. This, together with the use of cooled CCD cameras, online work stations and figures, brings us to applying this technique to a wide range of problems in materials science, solid state chemistry, mineralogy and condensed matter physics.

3. Basic principles

Conventionally, until the discovery of CBED, electron diffraction from a thin crystal in TEM was obtained using a method called selected area diffraction-(SAD). The geometry of electron diffraction is different in these two modes, namely SAD and CBED, as shown in figure 1.

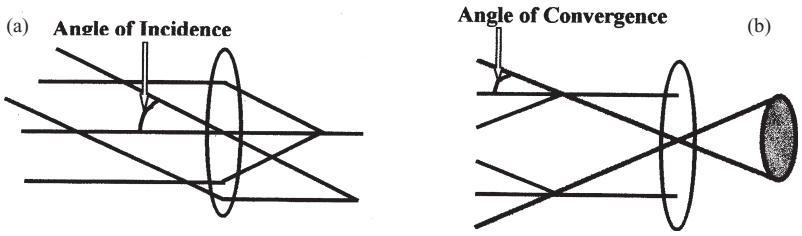

Figure 1. Electron diffraction in two different geometries. **(a)** Selected area diffraction (SAD) and **(b)** convergent beam electron diffraction (CBED).

It is seen that if a parallel beam of incident electrons is replaced by a convergent beam, diffraction spots of the SAD are enlarged into CBED discs. The same effect can also be introduced by rocking the specimen. In the former, the incident electron beam is a parallel beam of rays, with a single angle of incidence, α. In contrast, CBED makes use of a conical beam of electrons incident on the surface of the thin foil, with an angle of convergence as α. In such a case, the incident beam can be considered as a number of parallel incident beams, with a range of angles of incidence, from $-\alpha_i$ to $+\alpha_i$. In SAD, the area from which the diffraction information is collected is selected by introducing a mechanical aperture in the image plane. The demagnetized size of the aperture on the specimen plane defines the area from which diffraction information is collected. The smallest area from which diffraction information can be obtained using SAD is limited to 500 nm due to the spherical aberration of the objective lens and of the aperture (Leopold 1947). In CBED, the area for diffraction is chosen by focusing the incident beam into a very fine spot (2 nm) on the region of interest. The angle of convergence is altered by changing the size of the condenser aperture. In both the cases, the diffraction pattern is formed at the back focal plane (i.e.) of the objective lens, which is further magnified by a set of projector lenses. There is yet another mode of electron diffraction called the 'microdiffraction', in which the angle of incidence is in between that of SAD and CBED. The different modes of diffraction are identified by the relative value of the angle of convergence, α, to the Bragg angle of diffraction, θ_B, which is shown in figure 1. It is also clear that the angle of convergence, α, is proportional to the diameter of the diffraction disc in the diffraction pattern and the Bragg angle of diffraction θ_B, to the inter-spot/disc distance. These relations make it easy to calculate the angle of convergence experimentally. The comparison between the three modes of diffraction is summarized in table 1. The electron diffraction patterns in the three modes are shown in figure 2. It is clearly seen that SAD consists of a set of spots, while microdiffraction gives a set of discs of small angular range and the CBED pattern consists of a set of discs with a higher angular range.

It is observed from the geometry of diffraction that SAD and CBED patterns are obtained by interchanging the natures of the incident and the diffracted beams. That is, the incident beam in the case of SAD is a parallel beam, a disc of electron beams incident on the thin foil and all the diffracted beams are spots. In CBED, the incident beam is a spot on the surface of the thin foil, by virtue of the convergence introduced, and the diffracted beams are discs. Figure 3 shows the interchangeability of the incident and the diffracted beams in these two modes of diffraction, the principle of which is referred to as reciprocity theorem.

The spatial resolution of CBED is limited not by the size of the incident beam but by the broadening of the incident beam within the thin foil, especially in situations requiring diffraction information from thick sections of the thin foil, when these effects are dominant. For all practical purposes, the resolution can be taken as a few tens of nanometres.

Table 1. Comparison between different geometries of diffraction.

Convergent beam electron diffraction	Microdiffraction	Selected area diffraction
Small probe and large convergence	Small probe and very little convergence	Large probe size. No convergence
Large angular view of back focal plane of objective. So ZOLZ, FOLZ and HOLZ can be seen	Limited. Only ZOLZ and rarely FOLZ can be seen	Only ZOLZ
Finer details of intensity vs. angle θ due to crystal thickness and orientation differences within diffracting volume is not averaged	Intensity vs. θ is lost due to averaging effects	Information lost

ZOLZ – zero order laue zone; FOLZ – first order laue zone; HOLZ – high order laue zone

When a gradual change in the geometry of diffraction is introduced from CBED to SAD, certain features emerge. The centres of the CBED discs coincide with the spot pattern, when the angle of convergence is decreased and a parallel incidence case is approached. It is known that thickness and orientation are crucial in determining the intensity of diffracted electrons.

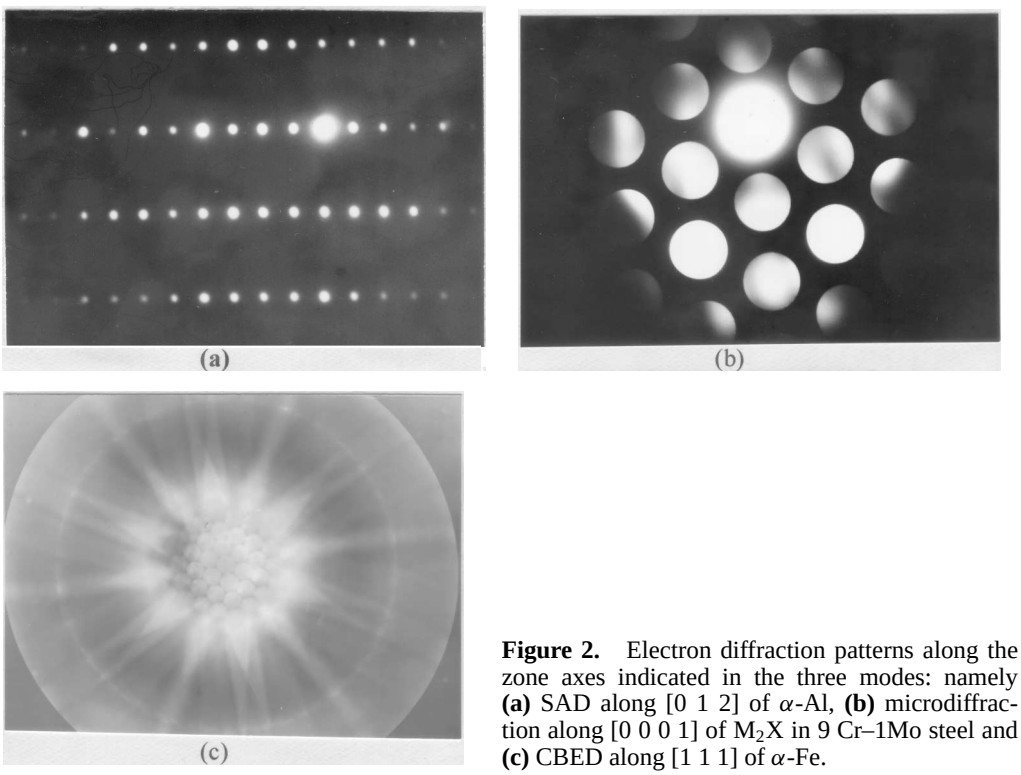

Figure 2. Electron diffraction patterns along the zone axes indicated in the three modes: namely **(a)** SAD along [0 1 2] of α-Al, **(b)** microdiffraction along [0 0 0 1] of M_2X in 9 Cr–1Mo steel and **(c)** CBED along [1 1 1] of α-Fe.

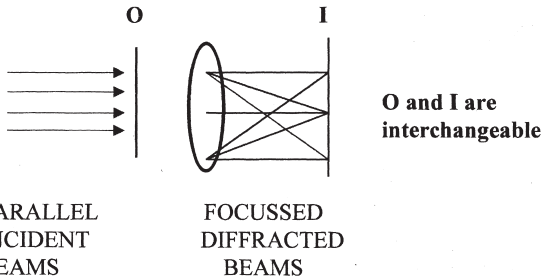

Figure 3. Reciprocity theorem illustrating the interchangeability of the incident and diffracted beams.

When the probe diameter is large, the variation in thickness and orientation within the illuminated area become so large that the useful information gets averaged out. This problem has been overcome with the finer probes available. In CBED, the incident convergent beam can be imagined as consisting of a large number of parallel beams. In such a case, for each parallel beam, a diffraction spot is formed at the back focal plane of the objective lens, but away from the optic axis. The distance of the diffracted spot from the optic axis depends on the inclination of the parallel beam under consideration. For every parallel beam, which contributes to the convergent beam, a diffraction spot is formed, depending on the angle of incidence. Thus, the intensity distribution within the CBED disc provides information about the angular dependence of diffracted intensity on the angle of incidence. Thus, the intensity distribution within each of the CBED discs is a two-dimensional map of diffracted intensity as a function of the inclination between the incident electrons and a particular crystal direction. For every point in the (0 0 0) disc of the CBED pattern, there is a corresponding point in every other diffracted disc, satisfying Bragg's law.

4. Additional information in CBED

The phenomenal developments in the field of processing of metastable, novel microstructures has offered challenging tasks in the unambiguous characterization of complex structures. Many available techniques need to be used in complementary ways to solve problems in structure analyses. Despite the development of techniques to identify structure, composition and morphology simultaneously, the literature abounds with examples of cases, where unique identification has been difficult. Distinguishing a spinodal product from a Guiner–Preston (GP) zone (Acuna & Bonfiglioli 1974), metastable phases like $M_{23}C_6$ and M_6C in ferritic steels (Tanaka *et al* 1983a), voids and bubbles produced during irradiation (Brown & Mazey 1964; Van Veen *et al* 1981), presence of low volume fractions of metastable fine δ-ferrite in a martensite matrix (Vijayalakshmi *et al* 1999) are some typical examples.

CBED has been able to successfully solve some of the problems mentioned above. The distinction of $M_{23}C_6$ from M_6C is illustrated here. Both the crystals have a face-centred cubic structure with lattice parameters of 1·08 and 1·12 nm respectively. These phases always form as minor constituents in steels (their amount $<$ 0·1%), preventing the application of other techniques like X-ray diffraction. The microchemistry of these carbides, even at equilibrium, can be quite varied depending on the chemistry of the steel. The lattice parameters are very sensitive to strain and composition. Though the equilibrium composition and lattice parameters are well-documented, their validity for metastable phases is questionable. The only difference between the two phases, in all stages of their evolution, is the crystal symmetry: $m3m$ for $M_{23}C_6$ and $d3m$ for M_6C. Determination of the symmetry by CBED thus is the

only confirmatory test to distinguish between the two carbides, which are often encountered in steels. Another case where CBED alone is of help in distinguishing between two similar phases is detecting the presence of fine, metastable δ-ferrite in a martensite matrix. This makes use of the measure of locked-in lattice strain in the two crystals, with much less strain in δ-ferrite compared to that in martensite.

Detailed analyses of CBED patterns could give good amount of additional and useful information about a crystal. These include (i) three-dimensional information about the reciprocal lattice, (ii) point and space-group symmetry details, (iii) lattice parameters from regions as fine as 2 nm, (iv) atom positions within a unit cell, and (v) defects in crystals. Each of these is discussed in detail below.

4.1 *Three-dimensional information about the reciprocal lattice*

Generally, in electron diffraction, it is known that there are three equivalent methods to represent the conditions for diffraction to take place: the Bragg's law; Laue conditions and construction of the Ewald sphere (Kittel 1976). The last method is geometrical in nature. The reciprocal lattice points which lie on the surface of an imaginary sphere of radius $1/\lambda$, (λ is the wavelength of the incident beam) satisfy the condition for constructive interference and intensity maximum occurs at these angles (figure 4). The shape of the diffraction peaks depends on the size of the diffracting crystal and the angular width is inversely proportional to the dimension of the diffracting crystal. Generally, the dimension of the thin foils used for transmission electron microscopy along the 'z' direction is too small (thickness $\sim$ a few nm). Hence, the angular widths of the diffraction peaks are large along the 'z' direction and show 'streaking' along the direction of the incident beam. All the diffraction peaks obey the well-known 'zone equation' (figure 4) and the reciprocal layers are termed as either zero order laue zone (ZOLZ) or first order laue zone (FOLZ) and so on, depending on the value of 'N' in the zone equation.

In conventional SAD mode, the angular view of the back focal plane (b.f.p.) of the objective lens is generally confined to the ZOLZ. In the case of CBED, the angular view of the back focal plane of the objective lens is enlarged significantly, due to the additional lens provided in the condenser-objective system. The difference between the two modes of diffraction, with

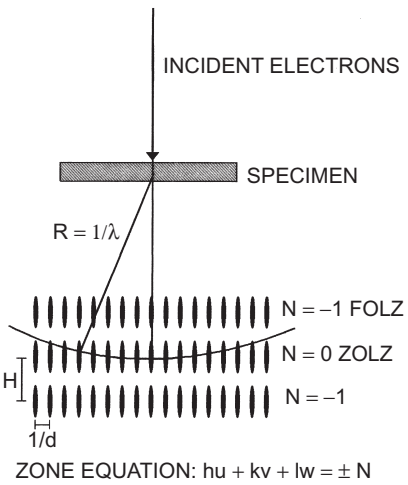

Figure 4. Plan view of Ewald sphere construction for electron diffraction. R represents the radius of the Ewald sphere, λ is the wavelength of incident electrons, d is the interlunar distance, H is the reciprocal lattice layer distance, and ZOLZ, FOLZ, SOLZ refer to the zero, first and second order lauer zones respectively. The zone equation is the basis for this classification.

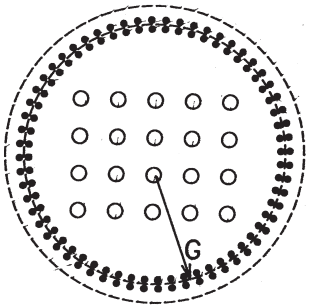

Figure 5. Sectional view of Ewald sphere showing radius of the FOLZ ring – G. H – reciprocal lattice layer distance, is related to G and λ.

respect to visibility of the b.f.p., of the objective lens, has already been illustrated in figure 2. The inter-zone distances are so small that their projection onto the observation plane can be assumed to retain the geometrical relations between H, λ and **G** (figure 5). The plane of observation is usually the plane in which the diffraction pattern is recorded using the photographic plate. A CBED pattern thus obtained, using a large angle of convergence from a large unit cell, consists of the following features: ZOLZ, whose discs are observed at the centre, zero intensity for short angular distances, corresponding to the curvature of the Ewald sphere between the ZOLZ and FOLZ, FOLZ which appears as a circle of discs which is actually the projection of the intersection of the Ewald sphere on the FOLZ. The same pattern repeats for SOLZ, HOLZ etc. A typical pattern is shown in figure 6. The inter-disc distances in the ZOLZ when analysed exactly along the same lines as that of SAD provides information regarding the two-dimensions of the reciprocal lattice. The corresponding two dimensions of the direct lattice can be derived from this information. Geometrical relations exist between the interlayer distances, diameter of the FOLZ and the third dimension of the reciprocal lattice of simple crystals like face-centred cubic, body-centred cubic etc. Using these relations, the third dimension can also be derived. Raghavan *et al* (1983), have used this principle to arrive at the complete description of the unit cell using a single CBED pattern.

4.2 *Point and space-group symmetry details*

The CBED pattern is a two-dimensional projection of the three-dimensional symmetry around a crystal axis, along which the electron beam is incident. The CBED pattern symmetries can be

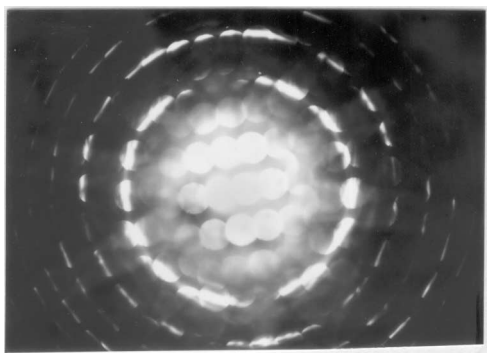

Figure 6. A typical CBED pattern along [0 6 $\bar{6}$] ZA of Al_6Mn showing HOLZ rings to derive three-dimensional information about the reciprocal lattice (ZA = zone axis).

described (Buxton *et al* 1976) by the 31 diffraction groups, which are isomorphic with Shubnikov groups. The relations between the diffraction groups and the point groups of crystals are also well-established. Hence, determination of the point group of a crystal, involves the following steps: (i) identification of diffraction group of the crystal, along one close-packed direction by study of the CBED pattern (figure 6) for whole-pattern symmetry, bright-field symmetry and dark-field symmetry along $+\mathbf{g}$ and $-\mathbf{g}$ directions; (ii) repetition of the same, if required, along different zone axes, and (iii) derivation of the point group symmetry of the crystal, based on diffraction symmetries. A number of references and illustrations are available in the literature (Stoter 1981; Steeds & Vincent 1983a; Tanaka *et al* 1983b) for the above application.

Space-group determination is carried out using the dynamical nature of electron diffraction. When a crystal has a screw axis or glide planes, forbidden reflections occur near the kinematical condition of diffraction. These have finite intensities when dynamical conditions of diffraction are operative. However, the cancellation of intensities, leading to extinction is still caused for certain directions of the incident beam. Such an effect appears as dark lines in the CBED discs that are called dynamic extinction lines or Gjonnes-Moodie (GM) lines. The dynamic extinction effect is similar to the interference phenomenon in the Michelson interferometer. That is, the incident beam is split into two beams by Bragg reflection in a crystal. These beams follow different paths, in which they suffer a relative phase shift when reflected by crystal planes, and are then superposed on a kinematically forbidden reflection to cancel each other out. Detailed methods to determine space groups from these lines are discussed in many references (Steeds & Vincent 1983b; Tanaka *et al* 1983a). The details in the CBED pattern are very sensitive to strain, defect and imaging conditions. Very often, these factors lead to error in judgment of the diffraction symmetries. Therefore, sufficient precaution must be taken while carrying out this exercise.

4.3 *Determination of lattice parameter*

The lattice parameter from microscopic regions is measured using CBED by making use of certain fine features of the pattern called the high order laue zone (HOLZ) lines (Jones *et al* 1977). These lines appear as a pair called "deficiency lines" and "excess lines" (figure 7). The deficiency lines are seen in the (0 0 0) disc of the CBED pattern and the corresponding 'excess' lines are seen in the discs of FOLZ. A pair of lines corresponds to a particular set of (*h k l*) planes of the crystal. The direction of these pair of lines is always parallel to each other. The origin of HOLZ lines, procedure for imaging the HOLZ lines, precautions required while imaging, indexing of these lines and factors that govern the position of HOLZ lines are discussed elsewhere (Vijayalakshmi 1997). The most important feature of relevance to the present discussion is that the angular position of these lines is sensitive to the accelerating voltage and the lattice parameter. Hence, if the accelerating voltage of the incident electrons is maintained constant, the changes in the angular position of these HOLZ lines can be directly correlated to the variations in the lattice parameter.

CBED has been found to be the most appropriate technique in this laboratory for the study of two problems, namely evaluation of lattice strain in microscopic regions (Vijayalakshmi 1997; Saroja 1999) and the study of point defects in ion-irradiated crystals (Vijayalakshmi 1997). A brief description of the first study is presented in the next section and the second study later.

4.3a *Lattice strain measurements using CBED:* The application of CBED for the identification and measurement of lattice strain in microscopic regions has been established (Spence

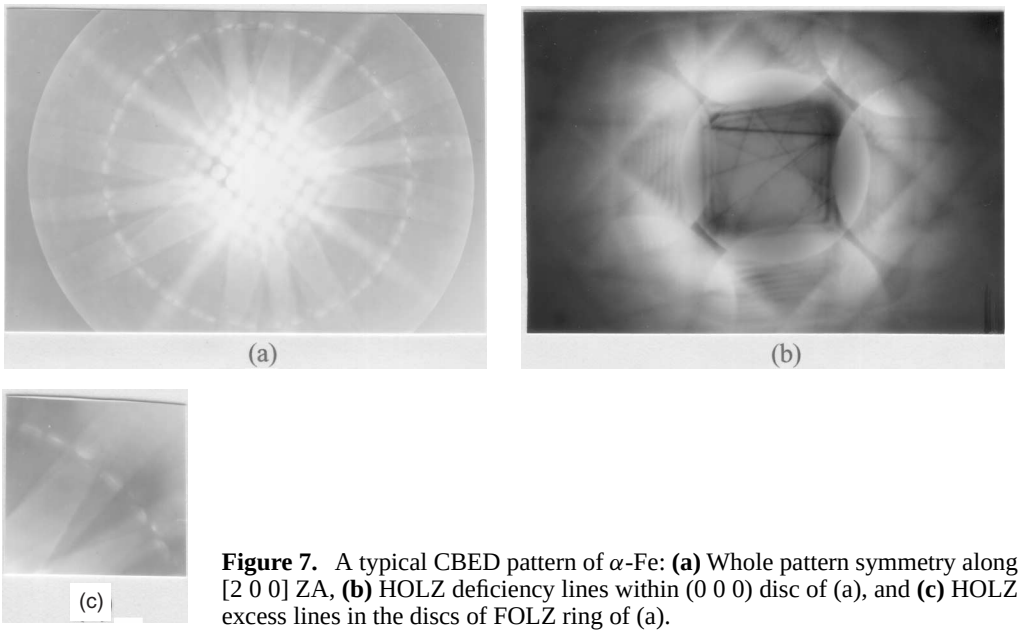

Figure 7. A typical CBED pattern of α-Fe: **(a)** Whole pattern symmetry along [2 0 0] ZA, **(b)** HOLZ deficiency lines within (0 0 0) disc of (a), and **(c)** HOLZ excess lines in the discs of FOLZ ring of (a).

& Zuo 1992). The method has been standardised for 9Cr–1Mo steel in wrought and welded conditions.

CBED patterns were obtained from the ferrite regions of 9Cr–1Mo steel with varying degrees of lattice strain due to their different thermal histories. In the case of weldment, the lattice strain variations with distance from the fusion zone were studied. The weldment was divided into four regions, the weld region, the heat-affected zone (HAZ) near the weld region, the HAZ close to the base metal and the base metal (figure 8). The percentage of change in the uniform lattice strain was evaluated from the shift in the angular position of HOLZ lines in the CBED pattern (figure 9), taken along the same zone axes, from the four regions under identical experimental conditions. Indexing of the HOLZ lines was done using EMS software. The distance between two chosen points on the HOLZ lines from the centre of (0 0 0) disc is measured and this distance is a measure of the change in the lattice parameter with respect to a reference (crystal with no strain). The detailed procedure for evaluation of lattice strain is given elsewhere (Vijayalakshmi 1997; Saroja 1999). The results obtained using CBED were compared with the X-ray FWHM values.

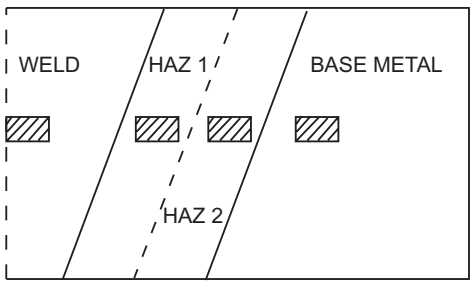

Figure 8. Schematic representation of the regions selected for study of variation of lattice strain by CBED experiments.

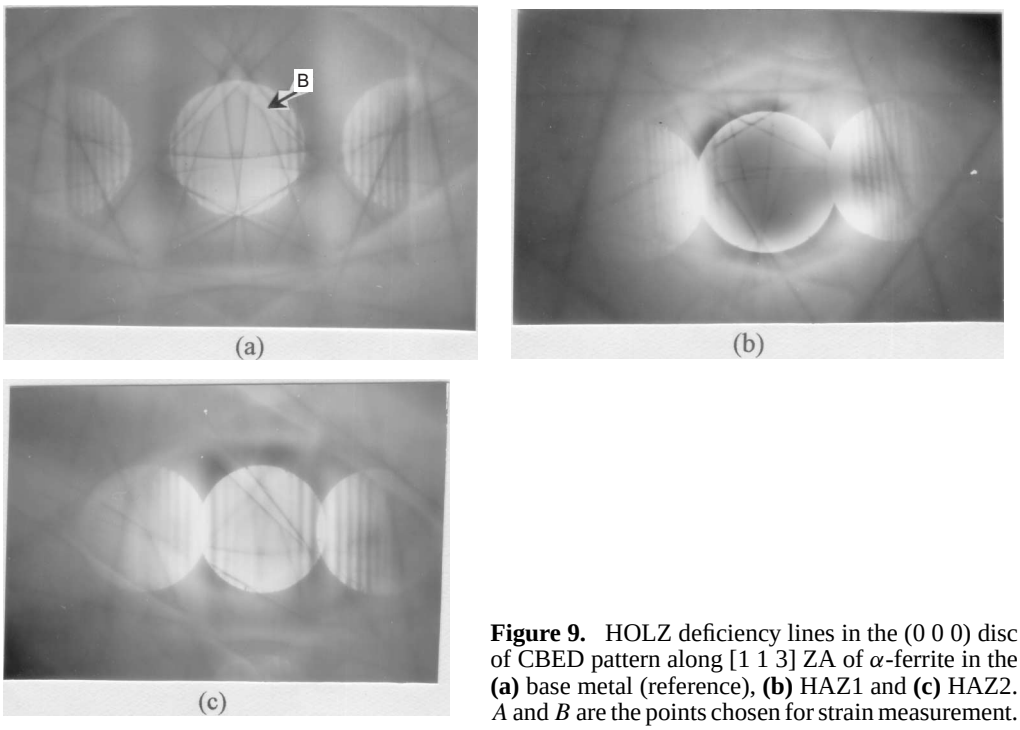

Figure 9. HOLZ deficiency lines in the (0 0 0) disc of CBED pattern along [1 1 3] ZA of α-ferrite in the **(a)** base metal (reference), **(b)** HAZ1 and **(c)** HAZ2. *A* and *B* are the points chosen for strain measurement.

4.4 *Atom positions within a unit cell*

For many decades, it was believed that electron diffraction is inferior to X-ray diffraction in providing quantitative information on diffraction intensities (Cowley 1978b). This limitation of electron diffraction was found to be due to the strong interaction of electrons with the scattering elements, namely the electrons of the atoms in the diffracting crystal. This has been termed the 'dynamical diffraction' effect. The consequence of the strong interaction of electrons with matter is that a one-to-one correlation could not be obtained between the scattering event and the intensity of diffracted beam, along a particular direction. As a result, no quantitative information could be obtained using electron diffraction, like the exact position coordinates of atoms within the unit cell of the crystal.

In order to obtain the above information, which is the ultimate in solving a crystal structure, intensity of diffraction under kinematical condition or weak scattering limits are required. The characteristics of diffraction depend on the ratio of the values of the scattered and incident energies. If the scattered energy is very small relative to the incident energy, one can regard the wave field after diffraction to be simply the addition of the incident, unperturbed wave and the scattered radiation. This is called the 'Born approximation' or the 'kinematic condition' of diffraction (Williams & Barry Carter 1996). X-rays and neutrons, by virtue of weak interaction with matter, are kinematic in nature and therefore provide diffraction intensities under kinematic conditions. Hence, the procedure for determination of atom positions has been developed in the early part of the last century, for X-ray and neutron diffraction. However, in the case of electrons, the scattering is strong and the 'Born approximation' breaks down.

In the case of CBED, it is already shown that the larger visibility range of b.f.p. of the objective lens provides information about intensity of diffraction about HOLZ discs. It is also

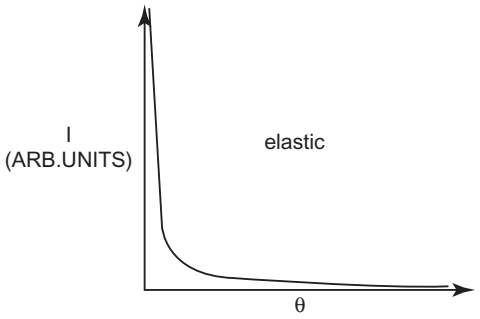

Figure 10. Angular distribution of the intensity of elastically, scattered electrons.

known that the intensity of diffraction reduces as the scattering angle increases. Figure 10 illustrates the angular dependence of scattered intensity vs. angle of scattering. Hence, the intensity of CBED discs at distances away from the optic axis or at very high angles of scattering is kinematic in nature and can be used to extract information about the atom positions. The method developed using CBED for the determination of atom positions makes use of this particular principle (Vincent *et al* 1984).

Figure 7 shows the 'excess lines' in FOLZ discs. The intensity of many of these lines corresponding to many (*h k l*)'s is recorded and visually arranged as per their relative intensities of diffraction. Such information provides the database for the proposed exercise of identifying the atom positions. A detailed analysis of the origin of these 'excess lines' is carried out to identify the 'Bloch states' that are responsible for their intensities and their relative strengths of excitation. This information is translated into the required data by detailed computation, the details of which are given elsewhere (Ichimiya & Uyeda 1977).

4.5 *Defects in a crystal*

CBED has been extended for the analysis of planar defects like stacking faults, twin boundaries and grain boundaries. The detailed analysis of line defects like dislocations has also been successful, using large angle CBED – LACBED (Tanaka *et al* 1980; Tafto & Metzger 1985). The present section discusses briefly the signature in CBED patterns, due to the presence of point defects, developed in the author's laboratory.

CBED patterns from perfect crystal contain two fine features that show signatures of point defects. These features are: (i) the 'interference pattern' within the (0 0 0) disc of a perfect crystal (figure 11), and (ii) the number of HOLZ rings (figure 6). It is to be kept in mind that the CBED pattern from a perfect crystal is a map of intensity of diffracted electrons. The three-dimensional crystal potential (figure 12a) can be considered as a projected two-dimensional potential (figure 12b) called the "string potential". The projection scheme is valid since the time available for the high energy, incident electrons, between the two parallel planes of atoms of the crystal, is very small. The strong interaction of the incident electrons with such a two-dimensional potential excites a number of plane waves called the "Bloch States" (figure 12c), the nature of which determines the intensity of diffraction. The 'interference pattern' within the (0 0 0) disc of a perfect crystal is caused by interference between the strongly excited "Bloch states". The second signature, namely, the number of HOLZ rings in a perfect crystal is also very high, since the crystal is defect-free and the inelastic scattering due to defects is practically minimum. The constituent atoms are in their equilibrium positions, leading to maxima in the strengths of the diffracted peaks. Thus, the signal to noise ratio is high, causing a large number of HOLZ rings to be imaged.

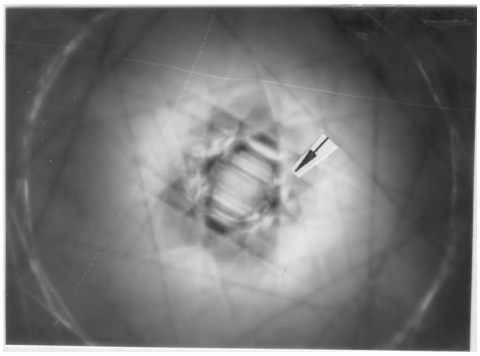

Figure 11. CBED pattern of α-ferrite along [1 1 3] ZA showing the interference pattern near the Brillouin zone boundary (arrow marked).

When point defects are introduced in a perfect lattice, by deformation, quenching or irradiation, the atoms are removed from their equilibrium positions and introduced in non-lattice positions. The lattice disorder reduces the strength of the periodic component of the scattering potential and therefore reduces the intensity of Bragg diffraction. Similarly, there is an increase in the diffuse background produced by elastic scattering from the aperiodic component of the crystal potential. The net result is to reduce the Bragg contrast, particularly for HOLZ reflections (figures 13a & b), which is associated with high-order Fourier coefficients in the scattering potential. The effect of increasing the Debye–Waller factor is two-fold: first, the string potentials (projected atomic potentials) become less sharp (figure 14a & b) thereby reducing the amplitudes for the HOLZ diffraction. The string potentials also become somewhat weaker, which induces some changes in the relative excitations and dispersions of the Bloch states (figures 15a & b), which contribute to the contrast in lowest order reflections. The overall contrast is reduced because the CBED discs are viewed against the diffuse background.

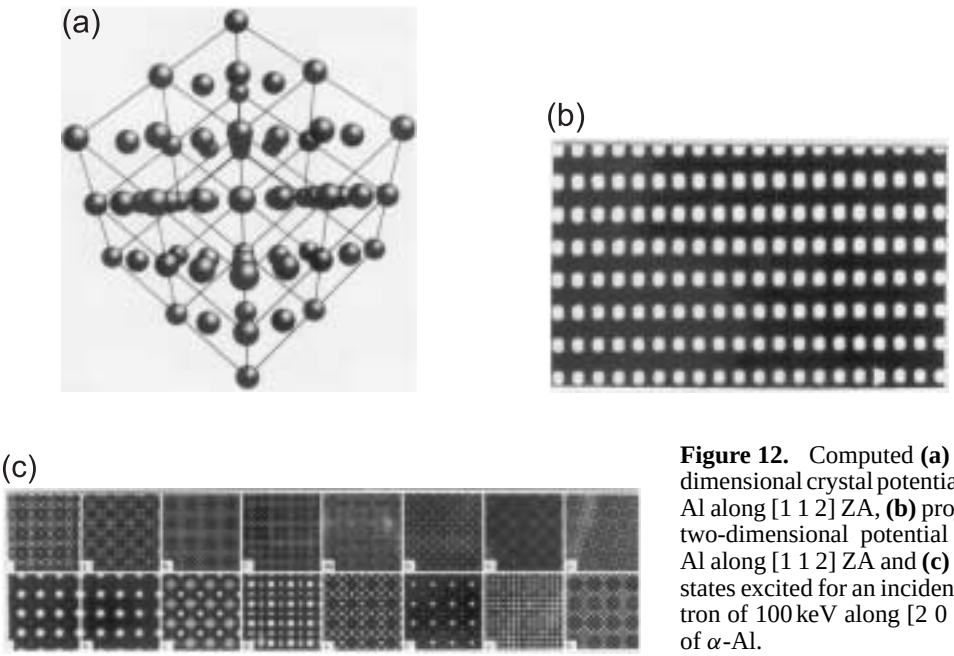

Figure 12. Computed **(a)** three-dimensional crystal potential in α-Al along [1 1 2] ZA, **(b)** projected two-dimensional potential in α-Al along [1 1 2] ZA and **(c)** Bloch states excited for an incident electron of 100 keV along [2 0 0] ZA of α-Al.

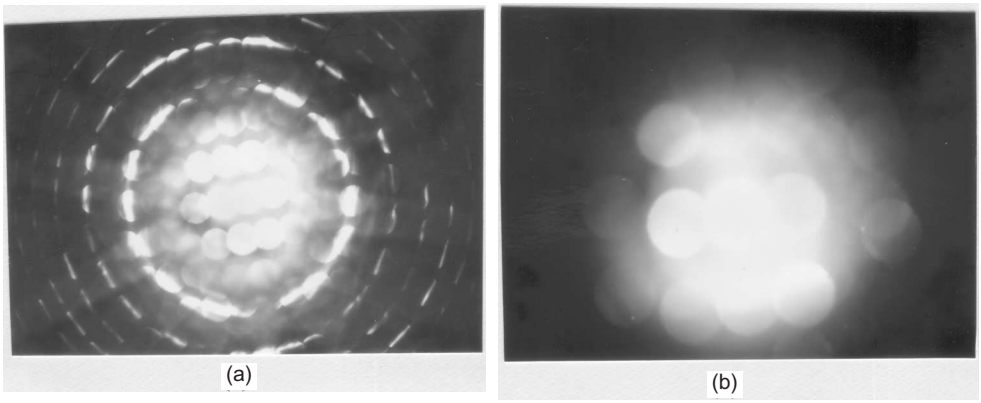

Figure 13. Reduction in the number of HOLZ rings in CBED patterns of Al_6Mn due to ion irradiation (100 keV argon ion): **(a)** unirradiated and **(b)** 2×10^{14} ions/cm^2.

The above effects can also be simply viewed in terms of increase in the Debye–Waller (D–W) factor due to increase in 'static mean square displacement'. The influence of increase in D–W factor as causing increase in inelastic scattering (noise) and reduction in elastic scattering signal is already very well-known. Hence, point defects increase the D–W factor and reduce the signal to noise ratio, leading to the observations stated above.

Thus, CBED patterns offer two signatures for the presence of point defects, which need to be quantified for estimation of their concentration. The application of CBED for identifying point defects is described below.

4.5a *CBED for identification of point defects:* The successful application of CBED for the identification of point defects has been demonstrated for the first time in this laboratory. The systems chosen are the weld of 9Cr–1Mo steel and Al-$14_{a/o}$Mn alloy, consisting of two phases, α-Fe and $M_{23}C_6$ in the first case and α-Al and Al_6Mn in the latter. Ion irradiation was chosen to introduce controlled amounts of point defects.

Two distinct features of CBED patterns that are sensitive to the concentration of point defects have been recognized. These are (i) the interference fringes in the (0 0 0) disk (figure 11) and (ii) the number of HOLZ rings (figure 6). These two features gradually reduce and disap-

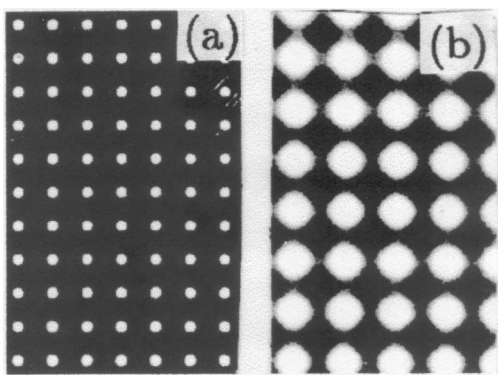

Figure 14. Smearing of projected potential along [2 0 0] ZA in α-Al, with increase in Debye Waller factor: **(a)** 0·005 and **(b)** 0·3 nm^{-1}.

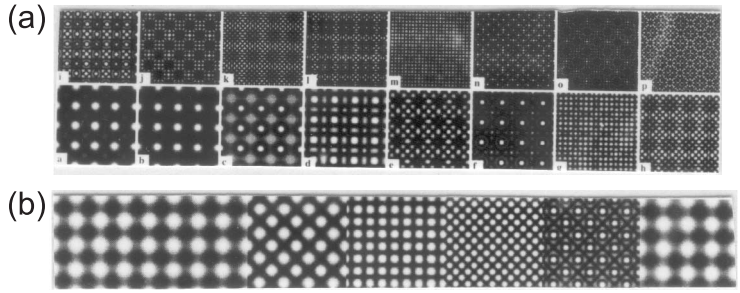

Figure 15. Smearing of Bloch states excited along [2 0 0] ZA in α-Al, for an incident electron of 100 keV, with increase in DW factor: **(a)** 0·005 and **(b)** 0·3 nm^{-1}.

pear with increase in dose, show unique dependence on the mass and energy of incident ions, and reappear on post-irradiation annealing. In order to identify the fundamental cause of the above observations, computations using EMS programs were carried out. These computations show that increase in the point defect concentration leads to smearing of projected potential, which in turn weakens and smears Bloch states that are excited. Consequently, the intensity oscillations of the interference pattern gradually disappear. The static displacement disorder reduces the strength of the large angle scattering, which is responsible for the reduction in the number of HOLZ rings. Thus the present studies describes identification of two distinct features sensitive to point defects and the understanding of the observed changes in terms of the projected potential, the excited Bloch states, the interference pattern in the CBED pattern, the static displacement disorder, the large angle scattering strength and the HOLZ rings.

4.6 *Thickness determination*

Sample thickness may be determined by a variety of methods in TEM like projected width of inclined stacking faults and EELS spectra (Egerton 1986). The popular CBED method (Kelly *et al* 1975) is based on the variation of the intensity of the diffracted beam with thickness known as 'Pendellosung' fringes. Under a two-beam condition, the measurement of excitation error at the positions of the fringe intensity minima can be used to determine the sample thickness, the method illustrated in several books on transmission electron microscopy (Spence & Zuo 1992; Williams & Barry Carter 1996). This method has been widely used by many material scientists today (Delille *et al* 2000; Bardal *et al* 2000) as this offers accuracy better than 2%.

5. Present status of CBED

In real materials defects, precipitates and local strains occur on a very fine scale so it became very essential to develop methods for obtaining smaller electron probes to minimize the contribution from defects, where conventional CBED fails. (Cowley 1978, 1992; Spence & Carpenter 1986; Brown *et al* 1988). The development of FEG (Tsong 1990) has contributed greatly to this. CBED patterns show high contrast as the probe size is reduced and further enhancement in contrast is obtained by using an energy filter tuned to the elastic peak in the energy loss spectrum (Lanio 1986). This could lead to improvements in critical-voltage measurements, lattice-parameter determination and in the resolution of branch cluster information (Midgley *et al* 1995; Kramer 2000). As the probe size becomes smaller, the electron beam

becomes fully coherent (Spence & Zuo 1992), which has led to the development of a variety of techniques for various problems in materials science. A few of them are discussed here.

5.1 *Nanodiffraction*

This is a special form of CBED, in which the emphasis is on obtaining diffraction patterns from regions of the specimen, about 1 nm or less in diameter. Unless a field-emission gun (FEG) is used, the intensity in a beam 1 nm in diameter is too small to be useful. Hence, nanodiffraction has been performed mainly in dedicated STEM instruments having cold FEG sources, although the newer TEM's with FEG's may also be used with efficient two-dimensional detector systems and recording with TV or CCD cameras (Cowley 1991). In the case of conventional CBED, the probe is incoherent and comparatively large. However, in nanodiffraction the electron beam is perfectly coherent with diameters as small as 0·2 nm, because of which crystallographic information on a near atomic scale can be obtained, with a wide range of applications. These include structure analysis of metal particles in catalysts (Cowley & Plano 1987; Pan *et al* 1987), study of defects (twins, dislocations etc.) and disorder in very small particles (Monosmith & Cowley 1984), use of HOLZ and Kikuchi line splitting to determine fault vector of the defect (Gjonnes 1985), structure of individual defects in thin crystal foils (Cowley *et al* 1984), determination of the local order in thin films of near amorphous materials or disordered crystals (Chan & Cowley 1981; Ohkubo *et al* 2000) and determination of local symmetry within particular parts of a unit cell of a crystal or a defect. A mixed mode operation of the microscope as in the convergent beam imaging (CBIM) and LACBED methods which produce a shadow image of the sample superimposed on the CBED pattern can also be used for the study of defects (Spence & Zuo 1992).

5.2 *Lattice imaging*

The discs in CBED patterns, formed using coherent nano probes with a large convergence angle are allowed to overlap, and the overlapping region of the pattern reveals the lattice fringes, which leads to STEM lattice imaging (Spence & Cowley 1978) (figure 16). It is possible to locate the probe accurately by this method at various regions within the unit cell and the CBED patterns obtained from these areas show different site symmetries (Ou *et al* 1989) and atomic positions. A coherent CBED pattern recorded with a very large objective aperture or without the objective aperture, so that a gross overlap of CBED discs occurs is called a 'ronchigram'. In fact, as an extreme case, if an ideal point source was available, an arrangement in the form of an '*X*' would produce an unaberrated lattice image of the crystal without using either lens or scanning. This point projection method for electron lattice imaging was proposed by Cowley & Moodie (1957). These resulting images are called Fourier images which are now being obtained even at very low accelerating voltages ($\sim$ 300 volts) using a sputtered tungsten field emission tip instead of a focused probe as a point electron emitter, without any lenses (Fink *et al* 1991).

5.3 *Electron holography*

Though invented in 1948 by Gabor, it came into prominence only in the 1990's. An electron hologram of an object is the interference pattern of the elastically scattered (diffracted) wave from the object and a reference wave, both resulting from a single primary wave and thereby achieving synchronism. The key feature of an electron hologram is that, unlike conventional TEM, both phase and amplitude of the beam can be recorded which enables us to study many phase dependent phenomena like magnetism (Tonomura 1987; Volkov & Zhu 2000;

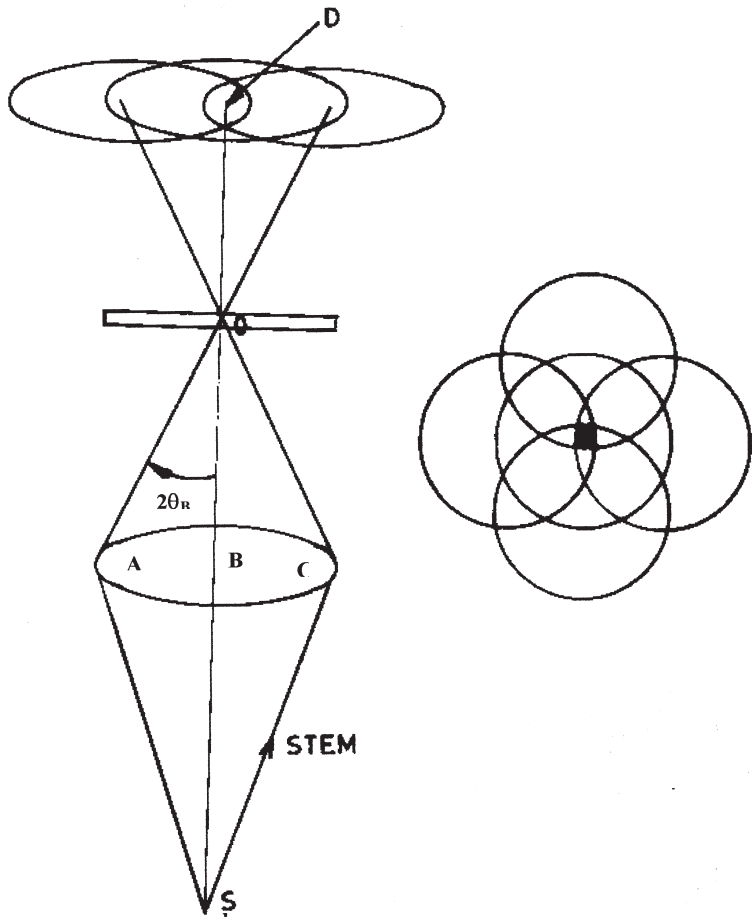

Figure 16. Axial three-beam lattice imaging in STEM, with an illumination angle twice the Bragg angle. Three orders overlap at *D*. The appearance of a two-dimensional coherent CBED pattern used for axial five beam imaging is shown at the right.

Shindo *et al* 2002) with a very high resolution. Several electron optical geometries have been developed for making electron holograms (Cowley 1992), but the most popular one is the "off-axis, image plane" geometry. It employs the electron biprism, invented by Möllenstedt and Düker in 1955. This device is simply an ultra-fine (0·3 μm in diameter) conductive fibre positioned in an imaging lens perpendicular to the electron beam so that it splits the field of view. A thin TEM specimen is placed over one side of the image field. When a positive voltage is applied to the fibre, the electron waves on either side of the fibre are bent toward the centre, eventually causing them to overlap. The overlapping waves create an interference pattern of parallel fringes. These fringes are changed in position and contrast, depending upon how the specimen affects the electron beam. The pattern is recorded either on film, or directly on to a digital CCD camera system. This interferogram, or hologram, is then processed to yield separate amplitude and phase images to give an atomic resolution (Orchowski *et al* 1995).

The coherent nano diffraction from thin crystals called the Gabor inline holography needs a point source and a weakly scattering transmission object. A number of reconstruction schemes

using coherent microdiffraction patterns are being attempted (Lehmann & Lichte 1995) Today electron holography has become a necessary tool in the study of nanocrystalline and magnetic materials (Beeli *et al* 1999), interfaces (Weiss *et al* 1993), heterostructures (Rosenauer *et al* 2001) and quantum wells (Cherns *et al* 1999).

6. Conclusions

The present paper is an overview on the technique of CBED summarizing various features like its discovery, historical development, principle, information obtained and its present status. The study of very small particles that could be as small as a single unit cell but could influence the mechanical and electrical properties of many technologically important materials like catalysts, microphases at interfaces etc. is not possible without a fine probe. Electron microscope instrumentation has undergone continuous developments for study of a wide range of materials problems. Today it is possible to observe directly the shape of electron orbitals and thus the shape of molecules. This is a very important step towards understanding chemical bonding, which holds matter together. Such information is of utmost significance not only for chemical science but also for applications related to materials properties, for example in the field of superconductors, semiconductors, nanomaterials, ceramics etc. Hence, it can be said with confidence that these advanced techniques and their development will pave the path for structure analysis problems for newer materials in future.

The authors wish to acknowledge the constant support and encouragement of Dr V S Raghunathan and Dr Baldev Raj.

References*

Acuna R, Bonfiglioli A 1974 *Acta Metall.* 22: 399
Bardal A, Lie K 2000 *Mater. Characterisation* 44 (3): 329
Beeli C, Doudin B, Ansermet J Ph, Stadelmann P 1999 *Mater. Characterisation* 42 (4–5) 175
Brown L M, Rodenburg J M, Pike W T 1988 *EUREM 1988* (London: Inst. of Physics) vol. 3, p. 93
Brown M, Mazey P 1964 *Philos. Mag.* 10: 1081
Buxton B F, Eades J A, Steeds J W, Rackham G M 1976 *Philos. Trans. R. Soc. London* A281: 271
Chan I Y T, Cowley J M 1981 *Proc. 39th Annual Meeting EMSA* p. 350
Cherns D, Barnard J, Mokhtari H 1999 *Mater. Sci. Eng.* B66 (1–3): 33
Cherns D, Kiely C J, Preston A 1988 *Ultramicroscopy* 24: 355
Cowley J M 1978a *Adv. Elect. Electron. Phys.* 46: 1
Cowley J M 1978b *Electron diffraction 1927–1977* (Bristol and London: Inst. of Physics) p. 156
Cowley J M 1991 *Electron Microsc. Soc. Am. Bull.* 57: 21
Cowley J M 1992 *Ultramicroscopy* 41: 335
Cowley J M, Moodie A F 1957 *Proc. Phys. Soc.* B70: 486
Cowley J M, Plano R J 1987 *J. Catal.* 108: 199
Cowley J M, Osman M A, Humble P 1984 *Ultramicroscopy* 15: 311
Crewe A V, Eggenberger D N 1968 *J. Wall Rev. Sci. Instrum.* 39: 576
Dellile D, Pantel R, Van Cappellen E 2000 *Ultramicroscopy* 87 (1–2): 5

*References in this list are not in journal format

Eades J A 1984 *J. Electron Microsc. Tech.* 1: 229
Egerton R F 1986 *Electron energy loss spectroscopy in the electron microscope* (New York: Plenum)
Fink H W, Schmid H, Kreuzer H J, Wierzbicki A 1991 *Phys. Rev. Lett.* 67: 1543
Gabor D 1948 *Nature (London)* 161: 777
Gjonnes J, Moodie A F 1965 *Acta Crystallogr.* 19: 65
Gjonnes J, Hoier R 1971 *Acta Crystallogr.* A27: 313
Gjonnes K 1985 *Ultramicroscopy* 17: 133
Gjonnes J, Hoier R 1969 *Acta Crystallogr.* A25: 595
Goodman P, Lehmpfuhl G 1968 *Acta Crystallogr.* 24: 339
Ichimiya A, Uyeda R 1977 *Z. Naturforsch.* A32: 750
Jones P M, Rackham G M, Steeds J W 1977 *Proc. R. Soc.* A354: 197
Kambe K 1957 *J. Phys. Soc. Jpn.* 12: 1
Kelly P M, Jostons A, Blake R G, Napier J G 1975 *J. Appl. Phys.* 62: 419
Kittel C 1976 *Introduction to solid state physics* (New York: Wiley)
Kossel W, Mollenstedt G 1939 *Ann. Physik* 36: 116
Kramer S 2000 *Ultramicroscopy* 81(3–4) 245
Lanio S 1986 *Optik* 73: 99
Le Poole J B 1947 *Philips Tech. Rundsch.* 9: 33
Lehmann M, Lichte H 1995 Holographic reconstruction methods. In *Electron holography:* ed. by A Tonomura, L F Allard, G Pozzi, Y A Ono, Elsevier Science BV (Proceedings of the Knoxville Workshop on Electron Holography), 69.
Lehmpful G, Reissland A 1968 *Z. Naturforsch* 23a: 544
Liu J, Hembree G G, Spinnler G E, Venables J A 1992 *Surf. Sci. Lett.* 262: 2111
MacGillavry C H 1940 *Physica* 7: 329
Marthinsen K, Hoier R 1986 *Acta Crystallogr.* A42: 484
Marthinsen K, Hoier R 1988 *Acta Crystallogr.* A44: 558
Midgley P A, Saunders M, Vincent R, Steeds J W 1995 *Ultramicroscopy* 59 (1–4) 1
Monosmith W B, Cowley J M 1984 *Ultramicroscopy* 12: 177
Moodie A F 1972 *Z. Naturforsch.* A27: 437
Newbury D E, Williams D B 2000 *Acta Metall.* 48: 323
Orchowski A, Rau W D, Lichte H 1995 *Phys. Rev. Lett.* 74: 399
Ou H J, Higgs A A, Cowley J M 1989 *Mat. Res. Soc. Proc.* 139: 223
Pan M, Cowley J M, Chan I Y 1987 *J. Appl. Crystallogr.* 20: 300
Raghavan M, Koo J Y, Petkovic-Luton R 1983 *J. Met.* 35 (6): 44
Rosenauer A, VanDyck D, Arzberger M, Abstreiter G 2001 *Ultramicroscopy* 88(1): 51
Saroja S 1999 *Study of microstructure, microchemistry and lattice strain in wrought 9Cr–1Mo steel using analytical transmission electron microscopy, convergent bean electron diffraction and thermodynamic computations.* Ph D thesis, University of Madras, Chennai
Shindo D, Park Y G, Yoshizawa Y 2002 *J. Magn. Magn. Mater.* 238: 101
Spence J C H, Carpenter R W 1986 Electron Microdiffraction In *Elements of analytical electron microscopy* (eds.) D C Joy, A Romig, H Goldstein (New York: Plenum)
Spence J C H, Cowley J M 1978 *Optik* 50: 129
Spence J C H, Zuo J M 1992 *Electron microdiffraction* (New York: Plenum)
Steeds J, Mansfield J 1984 *CBED of alloy phases* (Bristol: Adam Hilger)
Steeds J W, Vincent R 1983a *J. Appl. Crystallogr.* 16: 317
Steeds J W, Vincent R 1983b *J. Microsc. Spectrosc. Electron.* 8: 419
Steeds J W 1979 *Introduction to analytical electron microscopy* (eds) J J Hren, J I Goldstein, D C Joy (New York: plenum)
Stoter L P 1981 *J. Mater. Sci.* 16: 1356
Tafto J, Metzger T H 1985 *J. Appl. Crystallogr.* 18: 110
Tanaka M, Terauchi M 1985 *Convergent beam electron diffraction* (Tokyo: JEOL)
Tanaka M, Saito R, Ueno X, Harada Y 1980 *J. Electron Microsc.* 29: 408

Tanaka M, Saito R, Seiki H 1983a *Acta Crystallogr.* A39: 357
Tanaka M, Seiki H, Nagasawa T 1983b *Acta Crystallogr.* A39: 825
Tanaka M, Terauchi M, Kaneyama T 1988 *Convergent beam Electron diffraction II* (Tokyo: JEOL)
Tonomura A 1987 *Rev. Mod. Phys.* 59: 639
Tsong T T 1990 *Atom probe field ion microscopy* (New York: Cambridge University Press)
Uyeda R 1968 *Acta Crystallogr.* A24: 175
Van Veen A, Caspers L M, Evans J H 1981 *J. Nucl. Mater.* 103 & 104: 1181
Vijayalakshmi M 1997 *Application of analytical electron microscopy and convergent beam electron diffraction for the study of microstructural evolution in the weldments of 9Cr-1Mo steel.* Ph D thesis, University of Madras, Chennai
Vijayalakshmi M, Saroja S, Thomas Paul V, Mythili R, Raghunathan V S 1999 *Met. Mater. Trans.* A30: 161
Vincent R, Bird D, Steeds J W 1984 *Philos. Mag.* 50: 765
Volkov V V, Zhu Y 2000 *J. Magn. Magn. Mater.* 214: 204.
Warren J B 1979 *Introduction to analytical electron microscopy* (eds) J J Hren, J I Goldstein, D C Joy (New York: Plenum) p. 369
Williams D B, Barry Carter C 1996 *Transmission electron microscopy* (New York: Plenum)
Watanabe D, Uyeda R, Kogisco M 1968 *Acta Crystallogr.* A24: 249
Weiss J K, de Ruijter W J, Gajdardziska-Josifovska M, McCartney R 1993 *Ultramicroscopy* 50: 301
Zuo J M, Foley J, O'Keefe M, Spence J C H 1989 On the accurate measurement of structure factors in ceramics by electron diffraction In *Metal ceramic interfaces* (New York: Pergamon)